Materials Today Bio 32 (2025) 101732

Contents lists available at ScienceDirect

Materials Today Bio

journal homepage: www.journals.elsevier.com/materials-today-bio

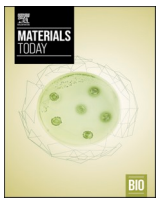

An exosome-based nanoplatform for siRNA delivery combined with starvation therapy promotes tumor cell death through autophagy, overcoming refractory KRAS-mutated tumors and restoring cetuximab chemosensitivity

Yurong Xiang [a,b,1], Qiang Liu [c,1], Kang Liu [d,1], Liuxian Chen [e,1], Fengjiao Chen [f], Tao Li [e], Siqi Li [a,b], Qiang Yu [a,b], Quan Lv [a,b], Zheng Xiang [a,b,*]

[a] Department of Gastrointestinal Surgery, The First Affiliated Hospital of Chongqing Medical University, No.1 Youyi Road, 400000, Chongqing, China
[b] Chongqing Key Laboratory of Department of General Surgery, The First Afiliated Hospital of Chongqing Medical University, No.1 Youyi Road, 400000, Chongqing, China
[c] Department of Hepatobiliary Surgery, Suining First People's Hospital, 22 Youfang Street, 629000, Suining, China
[d] Department of Cardiovascular Surgery, Fuwai Yunnan Cardiovascular Hospital, 528 Shahe North Road, 400042, Kunming, China
[e] Department of Key Laboratory of Molecular Biology for Infectious Diseases (Ministry of Education), Chongqing Medical University, No.1 Medical College Road, 400016, Chongqing, China
[f] Center for Clinical Molecular Medical Detection and Biobank, The First Affiliated Hospital of Chongqing Medical University, No.1 Youyi Road, 400000, Chongqing, China

ARTICLE INFO

Keywords:
Colorectal cancer
KRAS mutation
Starvation therapy
Exosome
Cetuximab chemosensitivity

ABSTRACT

Multi-drug combination therapy is one of the most effective strategies for the treatment of drug-resistant and advanced tumors. Modern nanodrug delivery systems are crucial for multi-drug combination therapy and gene therapy. However, research on direct injection of RNAi has not yielded significant results. Artificial vectors are emerging as promising delivery systemts for RNA for gene therapy. In this study, a multi-drug therapy system was built based on a biodegradable exosome nano-platform exploiting the protective and low immunogenic properties of exosomes for RNA. This work aimed to accomplish the co-delivery of siRNA and 3-Bromopyruvic acid (3BP) on an exosome nanoplatform, enhancing targeting by coupling cetuximab (CTX) to exosome membranes, resulting in a new nanomedicine Exo@siRNA/3BP-CTX (ERBC) engineered exosomes. The synthesis conditions were optimized to obtain stable, safe, and effective nanomedicines. Successful targeting of tumors with CTX inhibited KRAS oncogene expression and significantly reduced glucose uptake by cancer cells. This enhanced the starvation therapy effect of the energy deprivation agent 3BP, thus promoting excessive autophagy activation in cells and doubling apoptosis. However, ERBC combined with CTX therapy restored cellular chemosensitivity to CTX. These findings indicate that engineered exosomes with dual therapeutic activities is a promising approach for treating refractory KRAS-mutant cancers.

1. Introduction

The KRAS gene undergoes the most mutations in the MAPK pathway, accounting for 30 % of all human cancers [1]. KRAS mutation testing is routine in about 52 % of colorectal cancer (CRC) cases [2]. The mutants of CRC patients are associated with reduced sensitivity to chemotherapy and resistance to therapies targeting EGFR inhibitors, leading to an unfavorable prognosis. Additionally, patients with wild-type KRAS may develop subsequent mutations during anti-EGFR therapy, which confer resistance to EGFR inhibitors [3]. Notably, there are no effective drugs for treating KRAS mutations [4]. Tumors maintain proliferative signaling due to the continuous activation of driver oncogenes, such as KRAS. The siRNA can recognize specific messenger RNA (mRNA) sequences for silencing and is an effective potential therapeutic modality

* Corresponding author. Department of Gastrointestinal Surgery, The First Affiliated Hospital of Chongqing Medical University, No.1 Youyi Road, 400000, Chongqing, China.
E-mail address: 201876@hospital.cqmu.edu.cn (Z. Xiang).
[1] These authors contributed equally to this article.

https://doi.org/10.1016/j.mtbio.2025.101732
Received 19 January 2025; Received in revised form 1 April 2025; Accepted 4 April 2025
Available online 10 April 2025

for drug-resistant and untargeted genes [5,6]. Mutation-specific KRAS-siRNAs and broad-acting KRAS-siRNAs can selectively inhibit tumors relying on KRAS mutations for survival, with minimal toxicity [7,8]. Nonetheless, siRNAs may exhibit poor stability and inadequate pharmacokinetic properties and are vulnerable to degradation by nucleases in *vivo*. Besides, siRNAs are associated with a risk of eliciting off-target effects. Therefore, advanced siRNA-based therapeutics are needed to improve stability and targeting efficacy.

The activity of oncogenes is intricately associated with aberrant tumor metabolism and alteration of the tumor microenvironment [9]. Notably, tumor cells irreversibly favor glycolysis over oxidative phosphorylation as an energy source, even under aerobic conditions, an anomaly known as the "Warburg effect". Several intermediate metabolites produced during glycolysis provide raw materials for the proliferation of cancer cells [10]. Therefore, targeting glycolysis is an innovative approach for cancer therapy. The oncogenic KRAS gene can mediate this metabolic realignment by upregulating glucose transporter protein-1 (GLUT1), which enhances glucose uptake and glycolytic metabolism, allowing cells to survive under low-glucose conditions [11,12]. 3BP, a small molecule pyruvate mimetic and anticancer alkylating agent, possesses biocompatible anti-tumor properties. Besides, 3BP blocks the mitochondrial respiratory chain [13,14]. 3BP has a significant inhibitory effect on excessive glycolysis mediated by hexokinase-II (HK-II) overexpressed in tumor cells [15]. This leads to a collapse in adenosine triphosphate (ATP) production, resulting in a reduction in oxygen consumption and the restoration of oxygen levels that counteract hypoxia [16]. The respiratory inhibition of 3BP at low concentrations is significantly more effective than that of the conventional respiratory inhibitor 2-deoxy-D-glucose (2GD) [17]. However, the small molecular size of 3BP makes it difficult to be retained in tumor tissue due to enhanced permeability and retention (EPR) effects, limiting the direct application of 3BP in anti-tumor therapy [18].

Exosomes (Exo) are nanoscale lipid bilayer membrane vesicles with a diameter of 30~200 nm and are secreted by almost all cell types [19,20]. Exo contains many proteins, coding and noncoding RNAs, and lipids, which play important roles in intercellular communication and transport. Exosomes have several characteristics as carriers, including low immunogenicity, biodegradability, nontoxicity, strong cargo loading ability, and cargo protection. The use of exosomes as carriers for siRNA protects organelle stability and provides enough space for carrying 3BP simultaneously [21]. However, tumor-derived exosomes that naturally target tumors may not be optimal targets. Studies have shown that nucleic acids (RNA/DNA) and proteins can promote tumor development and metastasi [22]. Besides, selective membrane modification can overcome the disadvantage of the low targeting ability of natural exosomes.

EGFR, as one of the key factors driving cell proliferation, differentiation, and survival, is overexpressed in most colorectal cancer patients, providing a theoretical basis for the use of EGFR-targeted inhibitors (cetuximab, CTX) in the treatment of colorectal cancers [23]. CTX can be modified as a targeting antibody onto exosome membranes, with antibody-mediated endocytosis used to unload the drug for therapeutic effects [24,25]. CTX was approved by the Food and Drug Administration (FDA) in 2004 for the treatment of various tumors [26]. CTX has an affinity for EGFR receptors that is 5–10 times higher than that of endogenous ligands, effectively interfering with downstream signal transduction [27]. Notably, CTX has some acceptable side effects, such as rash, in patients, which rapidly recover. As a result, nano-drugs are being functionalized with CTX to enhance the targeting capabilities and synergistic therapeutic effects of drug delivery systems [28].

In the present study, ERBC-engineered exosomes selectively targeting EGFR-expressing tumor tissues were designed and synthesized. The dual-pathway anti-tumor mechanism of action is depicted in Scheme 1. The employed siRNA delivery platform for exosomes could effectively

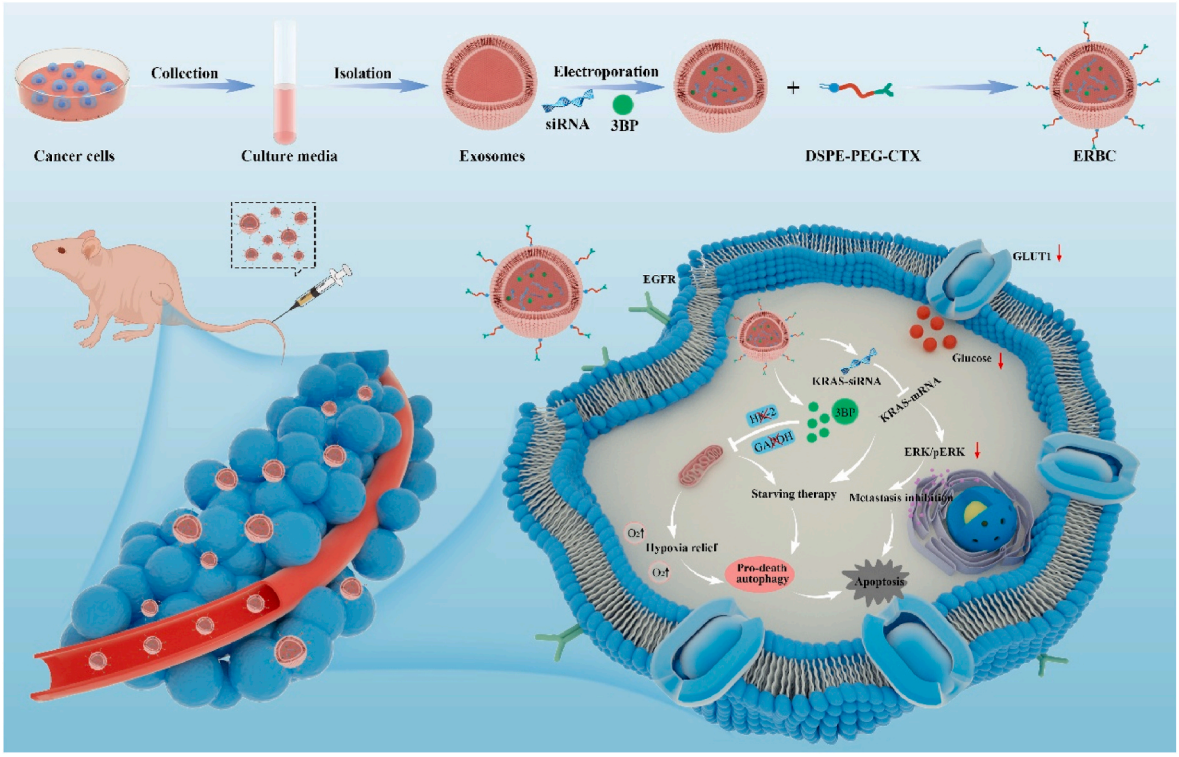

Scheme 1. Schematic representation of ERBC synthesis. First, the exosomes were loaded with siRNA and 3BP via electroporation. CTX was conjugated to HEK293T cell-derived exosomes via a click chemistry reaction to obtain ERBC nanomaterials. Extracellular vesicle targeting technology was used to deliver KRAS-siRNA to attenuate the aberrant expression of KRAS oncogenes, thus promoting proliferation and survival. Schematic representation of the mechanism by which ERBC enhances therapeutic efficacy to inhibit tumor metastasis and restore cetuximab sensitivity through EGFR-mediated entry into cells. This figure was drawn using Figdraw.

mitigate the instability and nonspecific targeting associated with unmodified siRNA, thereby ensuring stable gene silencing, re-establishing CTX sensitivity in KRAS-mutant CRC. This gene silencing modality diminishes the proliferation and viability of mutated cancer cells and also inhibits GLUT1 overexpression, thus attenuating cellular glucose uptake. Furthermore, 3BP was incorporated into the synthesis to synergistically enhance starvation therapy through direct energy inhibition. Besides, 3BP prolongs the survival of hormonal-treated mice due to the enhanced targeting ability, which reduces treatment side effects.

2. Experimental section/methods

2.1. Materials and reagents

Cell culture consumables were acquired from BIOFIL (China). RMPI 1640 medium, DMEM medium, and fetal bovine serum (FBS) were obtained from Gibco (Thermo Fisher Scientific, USA). 2DG and DSPE-PEG-NHs were sourced from Aladdin (Shanghai, China). Nuclear staining with DAPI, the fluorescent membrane dye DiI, the Annexin V-FITC/PI apoptosis detection kit, and RNase A were obtained from Beyotime Biotechnology (Shanghai, China). Themetabolic inhibitor 3BP and the CCK-8 were sourced from MedChem Express (China). CTX was sourced from MERCK (USA). A 300K Nanosep centrifugal device and AO/EB Staining Kit were sourced from Pall Life Sciences (USA) and Sangon Biotech (Shanghai, China), respectively.

2.2. Isolation, purification, and characterization of exosomes

Exosome-free FBS was prepared via ultracentrifugation (Beckman Coulter, USA) at 120,000×*g* for 16 h. Supernatants were collected from HEK293T cell cultures following standard protocols, then subjected to multistep gradient centrifugation to isolate exosomes [29–31]. The exosomes were then resuspended in 200 μl of PBS and stored at −80 °C for future use. The exosomes (100 μl) were diluted to 1 ml to measure the exosome concentration and hydrated diameter and analyzed via NTA (ZetaView, Particle Metrix, Germany). The protein content of the exosome suspension was quantified via the Bradford assay or the BCA assay, with BSA used as a standard. The same buffer was used for resuspending the exosome pellet. About 1–3 mg of exosomes was obtained from 500 ml of cell culture supernatant, according to the Bradford assay, corresponding to a concentration of 1.2×10^{11}particles ml^{-1} (NTA). Characterization of the exosomes, including morphological observations, was achieved via TEM (Tecnai G2 spirit Biotwin, FEI, USA). The presence of the exosomal markers CD63, Alix, CD9, TSG101 (from Abcam, UK), and pan cadherin (from Selleck, USA) was confirmed via Western blotting to confirm that the isolated vesicles were exosomes.

2.3. Exosome electroporation loading

Reagents and consumables were DEPC-treated before perforation to reduce the degradation of RNA enzymes. A preliminary experiment was conducted to determine the optimal parameters for loading siRNA and 3BP into exosomes, ensuring a suitable concentration and ratio alignment with system components [32]. siRNA: Exo of 1:18 and 3BP: Exo ratio of 4:1 were used for the follow-up experiments. The final concentration of exosomes in the mixture did not exceed 0.5 μg $μl^{-1}$ [33]. The appropriate proportional mixture was combined in 400 μl electroporation buffer (treated with PBS), followed by electroporation at 400 V, 125 μF, and ∞Ω using a Bio-Rad Gene Pulser (USA). The mixture was then immediately placed on ice [31,34]. The exosomes were then treated with RNase to eliminate any siRNA attached to the exosome surface [21]. The exosomes were diluted with cold PBS and centrifuged at 100,000×*g* and 4 °C for 70 min to remove unbound siRNA and 3BP. Cy3 fluorescence labeling was applied to the KRAS siRNA for fluorescence assays. Fluorescence assays were conducted to evaluate siRNA loading within Exo@siRNA-CTX or ERBC via a Multiskan MK3 microplate reader (Thermo Scientific, USA). Notably, 3BP exhibited a distinct absorption peak at 280 nm, according to a UV–vis spectrophotometer (UH5300 HITACHI, Japan). The loading factor was determined by measuring the concentrations of free 3BP and free Cy3-siRNA in the supernatants as follows: EE= (weight of loading in Exo/total weight of loading) × 100 %.

2.4. Preparation and characterization of ERBC

Cetuximab was conjugated to the surface of exosomes using DSPE-PEG-NHS [35]. Briefly, cetuximab was linked to DSPE-PEG-NHS by reacting it with N-hydroxysuccinimide (NHS) under alkaline conditions. The ratio of CTX to DSPE-PEG-NHS was maintained at 1:4 (W: W), and the mixture was stirred in MES buffer (pH = 8) at 80 rpm for 4 h at room temperature. The reaction mixture was mixed with exosomes at a 1:1 wt ratio based on the CTX mass standard to the exosome protein mass, then incubated at 37 °C for 2 h. Any unincorporated DSPE-PEG-CTX was removed through ultrafiltration via a 300 K Nanosep centrifuge. No significant CTX filtration was observed in the buffer after centrifugation after a 1:1 dropout ratio of CTX to exosomes. Four distinct types of cargo-loaded exosomes, including Exo-CTX, Exo@siRNA-CTX, Exo@3BP-CTX, and the dual-drug loading system ERBC, were synthesized using the method. Coomassie Brilliant Blue staining confirmed the successful self-assembly of CTX on the exosomes. The stability of the ERBC was assessed by measuring its size and zeta potential through NTA at 12 h, 24 h, and 48 h. NTA test was performed after the ERBCs were resuspended in a mixture containing PBS, 10 % FBS, and MES buffer (pH = 8.8).

2.5. siRNA transfection

Highly efficient KRAS siRNA oligonucleotides with the sequence (sense 5′-3':GGACUCUGAAGAUGUACCU[dT][dT]) have been detected [36]. In this study, oligonucleotides for KRAS CY3-siRNA, KRAS siRNA, and control negative siRNA (siNEG) oligonucleotides were sourced from Sangon Biotech (China). Lipofectamine ^{TM}3000 (Lipo ^{TM}3000) Transfection Reagent (Thermo Fisher Scientific, UK) was utilized to achieve a final siRNA concentration of 20 nM for comparison, following the manufacturer's protocol. The efficacy of siRNA-induced knockdown was evaluated via Western blot analysis 48 h post-transfection.

2.6. Uptake by in vitro cells

Control exosomes (blank exosomes) and ERBC were labeled with the cell membrane fluorescent probe Dil via incubation at 37 °C for 2 h. The samples were ultrafiltered thrice in a 300 K Nanosep centrifuge to remove free dye. Confocal laser scanning microscopy (Leica, Germany) and flow cytometry (Beckman Coulter, USA) were used to evaluate the uptake of DiI-labeled control exosomes and ERBC nanocarriers by SW480 or SW620 cells after 4 h of incubation.

2.7. Biodistribution of exosomes in vivo

The extracted exosomes were labeled with 5 μM DiR, a near-infrared fluorescent dye, at 37 °C for 30 min, and unincorporated (free DiR) was removed through ultrafiltration three times in a 300K Nanosep centrifugal device. When the tumors reached a volume of 150–200 mm^3, the mice were intravenously administered with 100 μl of DiR-ERBC or DiR-exosome control group nanomaterials equivalent to ~10^9 exosomes per rat. The *in vivo* fluorescence of the injected exosomes was monitored at specific time points via the Xenogen IVIS Spectrum system.

2.8. Cell viability assay

Cell viability was determined via the CCK-8 assay. Briefly, NCM460 or SW480 cells were seeded into 96-well plates (1×10^4 cells/well) and

subjected to various treatments for 48 h. For apoptosis analysis, SW480 cells were seeded in 24-well plates (5×10^4 cells/well), then treated with various agents for 48 h. Apoptosis was then assessed via an Annexin V-FITC/PI apoptosis detection kit, and the results were analyzed via flow cytometry.

2.9. Cell migration in vitro

First, SW480 cells were incubated in a medium containing 1 % FBS. The cells (2.5×10^4) were seeded with 100 μL of serum-free medium enriched with Exo-CTX, Exo@siRNA-CTX, Exo@3B-CTX, or ERBC in the upper chamber of a transwell while the lower chamber was filled with 500 μl of medium with 10 % FBS. The cells that migrated through the membrane to the lower surface after 48 h were fixed with 4 % paraformaldehyde and stained with 0.05 % crystalviolet. Cells within three randomly selected fields were counted. The cells were exposed to Exo-CTX, Exo@siRNA-CTX, Exo@3B-CTX, or ERBC (100 μg ml^{-1}) for 48 h, then a scratch was made in the monolayer of each well in triplicate. Images were recorded immediately after the scratch (0 h) and again at 48 h post-scratch. The degree of wound closure was determined based on the scratch area at both time points via ImageJ software to analyze the reduction in wound size.

2.10. Western blot

Total exosomes, cell and tissue proteins were isolated and lysed in the RIPA buffer. The concentration of the total protein was determined via a BCA protein assay kit. From each sample supernatant, 30 μg of total protein was separated by SDS–PAGE and subsequently transferred onto a PVDF membrane. The membrane was blocked with 5 % skim milk for 1.5 h. Protein bands were detected using ECL chemiluminescence. Band intensities were quantified with image analysis software, and the expression levels of the proteins were normalized to that β-Actin.

2.11. In vivo treatment and efficacy evaluation

When the tumors growth reached approximately 75 mm^3 in size, the mice were randomly divided into five groups: PBS, Exo@siRNA-CTX, Exo@siRNA-CTX + Free CTX, Exo@siRNA/3BP-CTX, and Exo@siRNA/3BP-CTX + Free CTX. The mice were intravenously injected with exosomes equivalent to ~10^9 exosomes per rat, and free CTX was administered at a concentration of 5 mg ml^{-1}. After 21 days of treatment, we assessed clinical indicators of heart and kidney function, including Alanine aminotransferase (ALT), Aspartate aminotransferase (AST), and Creatinine (CR). Tumor tissues and major organs were collected, sectioned, and subjected to histological and immunohistochemical analyses. H&E staining was performed, and immunohistochemical analysis focused on KRAS and Ki67.

2.12. Statistical analysis

Data are presented as the means ± SD (n = 3), and significant differences between two groups were analyzed using unpaired two-tailed Student's t-tests. Comparisons of parameters among three or more groups were made using one-way analysis of variance (ANOVA) for single-factor variables followed by Tukey's posthoc tests. No significant difference was denoted n.s., and statistical significance was denoted as $^*P < 0.05$, $^{**}P < 0.01$, and $^{***}P < 0.001$.

3. Results

3.1. Isolation and characterization of exosomes

Exosome, as natural liposomal bilayer nanocarriers, offer suitable spatial capacity for drug encapsulation and demonstrate exceptional biocompatibility *in vivo* [30,31,37]. Herein, parental exosomes were isolated from HEK293T cell (293T) culture supernatants via gradient centrifugation and ultracentrifugation. Transmission Electron Microscope (TEM) revealed that the exosomes had a distinct membrane structure and consistent size distribution. Nanoparticle tracking analysis (NTA) revealed that the exosome size was 122.84 ± 12.80 nm (Fig. 1a). Coomassie blue protein staining was used to distinguish exosome proteins and 293T cell membrane proteins (Fig. 1b). Moreover, Western blot revealed that the exosomes highly expressed Alix, CD63, TSG101, and CD9 (Fig. 1c). Flow cytometry (FCM) also revealed that the exosomes highly expressed CD63 and CD9 (Fig. 1d). However, Pan cadherin, a cell membrane surface molecule, was not expressed in the exosomes (Fig. 1c). Collectively, these findings indicate that exosomes were successfully isolated. The exosomes suitable for downstream applications were purified.

3.2. ERBC synthesis and characterization

Exosomes were co-loaded with KRAS-siRNA and 3BP through electroporation. siRNA was modified to Cy3 fluorescence (Cy3-siRNA) for better visualization of the siRNA for analysis. Cy3-siRNA relative fluorescence units (RFU) were measured via zymography. Cy3 fluorescence within the exosomes confirmed the successful incorporation of Cy3-siRNA (Fig. 1e) without compromising the integrity of the KRAS-siRNA structure (Fig. S1, Supporting Information) [33]. PBS was used as the electroporation buffer to better determine the loading rate. The linear curve between the siRNA concentration and Cy3 RFU (Fig. S2) showed that the encapsulation efficiency (EE) of the siRNA in Exo@siRNA/3BP was 21.40 %. The UV–vis absorption peak at 280 nm was visible in the supernatant after Exo@siRNA/3BP and Exo@3BP were super-isolated (Fig. 1f), indicating the UV–vis spectral concentration curve for 3BP (Figs. S3 and S4). The difference in concentration calculated from the UV–vis absorption values of 3BP before and after electroporation showed that the EE for 3BP in Exo@siRNA/3BP was 19.49 % [14,30]. DSPE-PEG-NHS, a polyethylene glycol-modified phospholipid with excellent amphipathic properties, was immobilized onto the exosome surface using DSPE-PEG-NHS as a linking agent to increase the tumor-targeting ability of the exosomes. CTX, a recombinant human/-mouse chimeric IgG1 mAb of about 152 kDa, breaks down into the light and heavy chains constituting the antibody upon denaturation [26,38]. Herein, Coomassie blue protein staining detected the characteristic bands of cetuximab at about 25 kDa and 55 kDa after centrifugation (Fig. 1g), indicating successful attachment of cetuximab to the exosome surface via PEGylation. TEM revealed that ERBC had the same shape and structure as unmodified control exosomes (Fig. 1h). Notably, NTA tests showed that the particle size was not significantly different between the exosome and ERBC (Fig. 1i). Compared with exosomes, the zeta potential of ERBC was more negative. Cetuximab altered the potential of the exosome surface (Fig. 1j). Protein blot analysis revealed that ERBC and exosomes had the same specific proteins (Fig. 1c). Further stability analyses revealed that the particle size or zeta potential of ERBC stored in 10 % FBS, PBS, or MES buffer at 4 °C for 48 h did not change (Fig. 1k and l), ensuring its integrity for subsequent use.

The uptake of the Exo@siRNA-CTX nanocomplex (Exo_{DiI}@$siRNA_{FITC}$-CTX) by SW480 cells was simultaneously tracked in *vitro* using confocal microscopy and FCM (Fig. S5). FCM results indicated that 63.83 % of SW480 cells exhibited positive uptake of Exo@$siRNA_{FITC}$-CTX at 48 h post-incubation at 37 °C. The uptake of $siRNA_{FITC}$ samples was minimal (3.36 %) (Fig. S5b). $siRNA_{FITC}$ alone, without exosome-mediated electroporation, exhibited negligible uptake. Confocal microscopy revealed colocalization of Exo_{DiI} (red) and $siRNA_{FITC}$ (green) at 4 h post-treatment, confirming the successful encapsulation of siRNA into exosomes via electroporation and demonstrating that siRNA internalization into cells was mediated by exosomes (Fig. S5c).

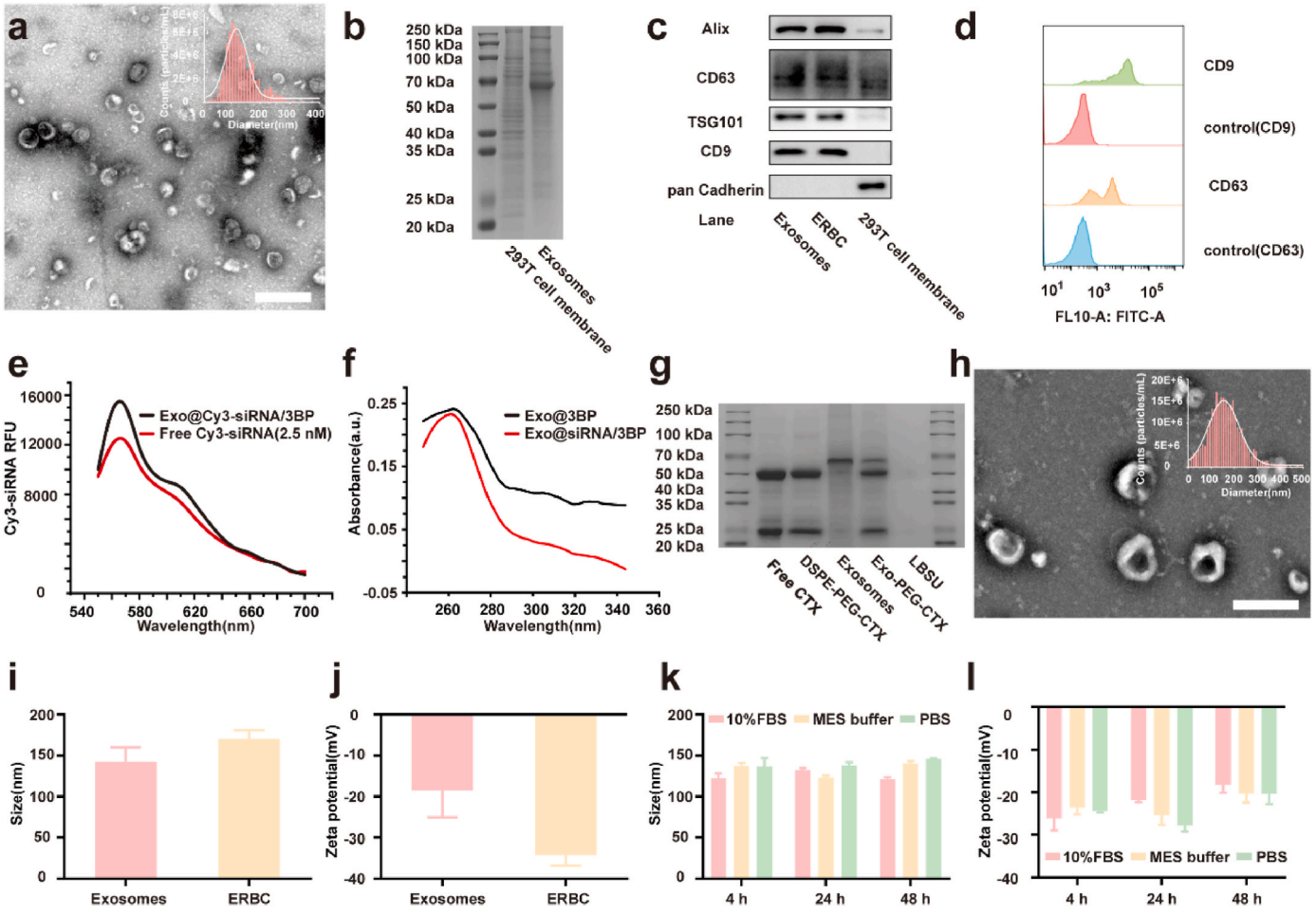

Fig. 1. Preparation of ERBC and characterization of exosomes. a) Representative TEM images of exosomes and size distribution of exosomes as determined by NTA, presented at a scale bar of 500 nm. b) Coomassie blue protein staining of the exosomes proteins and 293T cell membrane proteins. c) The expression of Alix, CD63, TSG101, CD9, and Pan Cadherin (ERBC markers) was quantified via Western blot. d) The FCM analysis of CD63 and CD9 exosome membrane surface protein expression; Event records 5000 polymers. e) RFU values recorded at 570 nm from the Cy3 fluorescence spectra of Exo@Cy3-siRNA/3BP and Cy3-siRNA as determined via the zymography technique. f) The UV–vis absorption spectra of 3BP. g) Coomassie blue protein staining map, LBSU: lower buffer solution after the first ultrafiltration. h) Representative TEM micrograph of ERBC. Scale bar: 200 nm. i) The size of the extracted particles in the ERBC and exosomes was determined by NTA. j) Nano-Sight analysis demonstrating the zeta potential of ERBC and exosomes. k), l) Changes in the size and zeta potential of ERBC stored in different buffers and serum for 4 h, 24 h and 48 h (n = 3). (For interpretation of the references to color in this figure legend, the reader is referred to the Web version of this article.)

3.3. *ERBC is highly targeted in EGFR-overexpressing tumors*

High drug levels at the tumor site effectively kill the cells and minimize systemic toxicity [35,39]. Herein, western blot analysis revealed that the SW480 colorectal cell line highly expressed the EGFR and KRSA proteins. The SW620 cell line, which does not express EGFR, was used as a control group for the experiment (Fig. S6). Confocal microscopy and FCM were used to assess the cellular uptake of ERBC and control exosomes. Notably, the cetuximab-modified ERBC exhibited significantly higher internalization rates in the SW480 cell line than in the SW620 cell line, while ERBC endocytic uptake was comparable to exosomes (Fig. 2a). The cellular uptake efficiency of ERBC in SW480 cells, which exhibit high EGFR expression, was 2.90-fold higher than that of pure exosomes. In contrast, in SW620 cells, which exhibit low EGFR expression, the uptake efficiencies of ERBC and pure exosomes showed no statistically significant difference (Fig. 2b). Similarly, FCM suggested that SW480 cells had the highest ERBC uptake (Fig. 2c). Viabilitytests revealed that the cytotoxic effect of ERBC was stronger on SW480 cells than on SW620 cells, possibly because of the targeting effect of ERBCs on SW480 cells (Fig. S7). DiR-labeled ERBC and exosomes were injected into mice via the tail vein, and near-infrared fluorescence signals were monitored using an in *vivo* IVIS. DiR fluorescence was detected throughout the body in all mouse groups at 4 h post-injection. In SW480 tumor-bearing mice, the ERBC-treated group exhibited the highest fluorescent signal accumulation at 48 h (Fig. 2e), with quantitative analysis showing an approximately 3.24-fold increase compared to the exosome-treated group (Fig. 2d). Notably, ERBC also partly accumulated at the tumor site in the mice bearing SW620 tumors. However, the control exosomes did not affect the tumor site distribution. The preferential aggregation at the tumor site may be due to the enhanced EPR, which is further facilitated by the prolonged circulation half-life of PEG-modified exosomes [40]. These findings demonstrated that ERBC exhibited extended in *vivo* circulation time and EGFR overexpressing tumor-targeting ability. Imaging of major ex *vivo* organs (heart, liver, spleen, lungs, and kidneys) revealed that exosome nanoparticles were predominantly aggregated in the liver and spleen (Fig. S8).

3.4. *Therapeutic Efficacy of In Vitro Treatment*

The effect of ERBC on cell viability was assessed using a live/dead assay. SW480 cells were first treated with exosome-based drug formulations for 48 h. The Exo@siRNA-CTX, Exo@3BP-CTX, and ERBC groups exhibited varying degrees of cell death (red fluorescence), with the

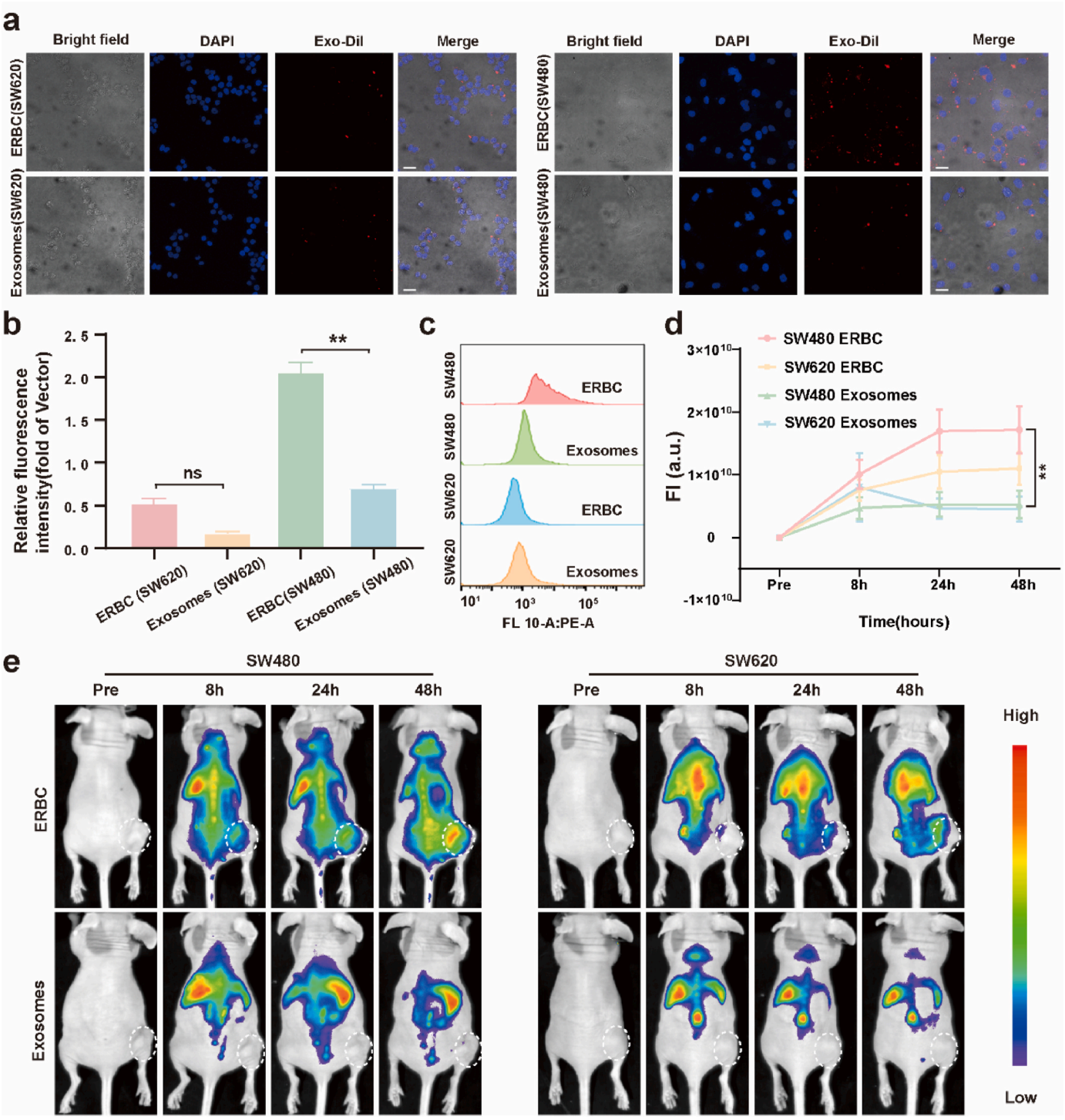

Fig. 2. In *vivo* and in *vitro* targeting of ERBC. a) The membranes of ERBC and control exosomes were stained with DiI and cocultured with SW620 or SW480 cells for 4 h. Real-time confocal images of SW620 or SW480 cells. Red fluorescence represents the DiI signal, and the nuclei were stained with DAPI (blue). Scale bar = 20 μm. b) Quantification of the mean fluorescence intensity of red fluorescence represents the DiI signal in Real-time confocal images of SW620 or SW480 cells (n = 3). The data are presented as the means ± SD. c) FCM analysis of DiI fluorescence signals in cells. Events per 10,000 cells. d) semiquantitative biodistributions of ERBC and Exosomes at different time intervals (n = 3). The data are presented as the means ± SD. e) In *vivo* IVIS imaging of mice after tail vein injection (~10^9 exosomes per mouse) with control exosomes or ERBC at fixed time points (8 h, 24 h and 48 h after injection). Two subcutaneous nude mice models were established with SW480 or SW620 cells. The white dotted lines indicate the tumor site (n = 3). (For interpretation of the references to color in this figure legend, the reader is referred to the Web version of this article.)

ERBC group showing the most pronounced effect (Fig. 3a). In *vitro* assessment of the viability of SW480 cells following various treatments was conducted via the Cell Counting Kit-8 (CCK-8) assay. Compared with Exo@siRNA-CTX treatment, the addition of free CTX (250 μg ml^{-1}) to the Exo@siRNA-CTX treatment group increased the cytotoxic response (Fig. 3b). After 48 h of treatment, the cell survival rate in the ERBC + Free CTX group was 27.06 %, whereas the cell survival rate in the ERBC-only group was 42.48 %.

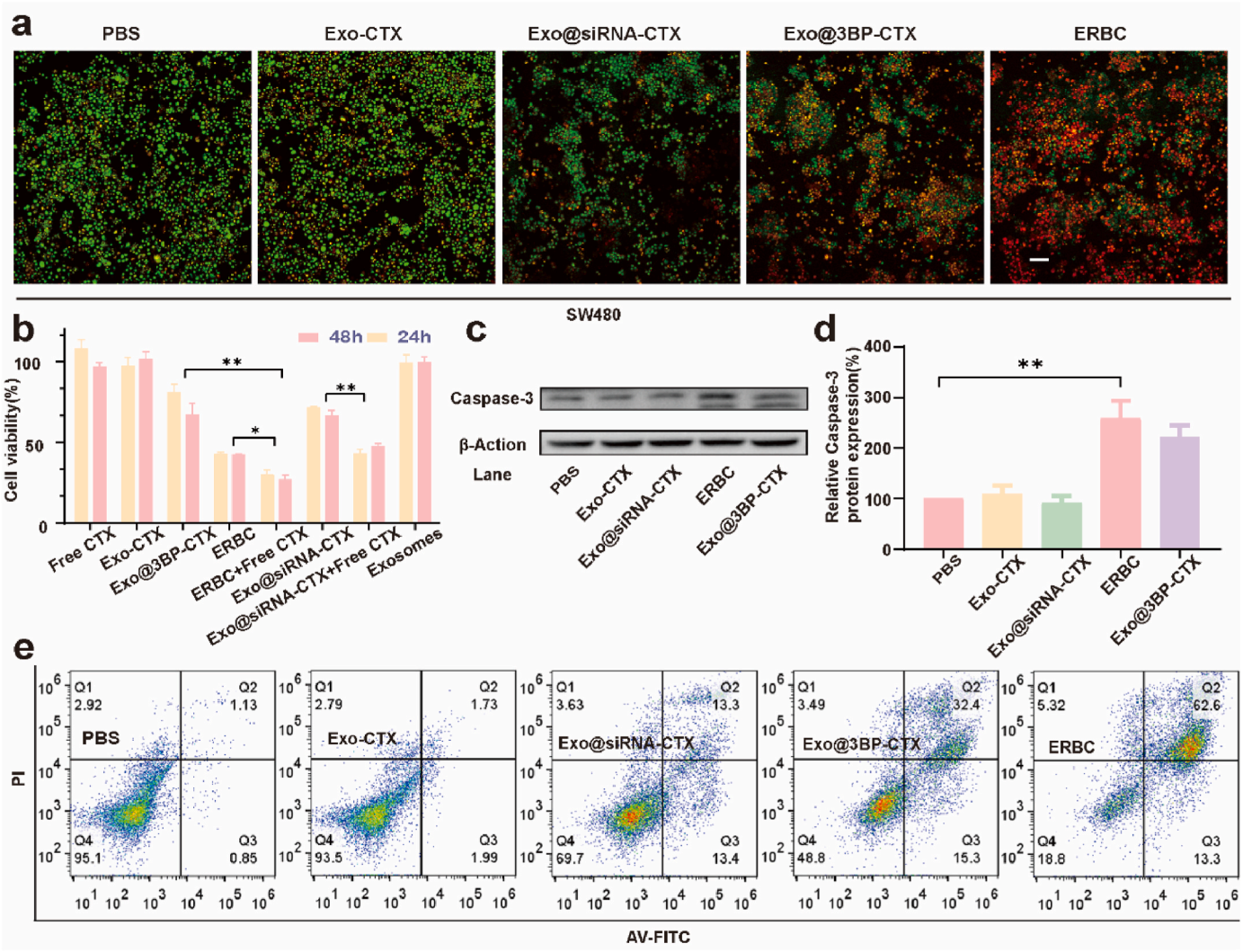

Fig. 3. Therapeutic efficacy of in *Vitro* treatment. a) Detection of live/dead cells via the double-staining assay with acridine orange (AO) and ethylpyridine bromide (EB) in the PBS, Exo-CTX, Exo@siRNA-CTX, Exo@3BP-CTX or ERBC nanovector groups; scale bar:100 μm. b) Analysis of the cytotoxicity of SW480 cells measured with the CCK-8 kit after treatment with PBS, Exo-CTX, Exo@siRNA-CTX, Exo@3BP-CTX, or ERBC, with or without free CTX (250 μg ml^{-1}). The date are expressed as the mean ± SD (n = 5). c) Western blot analysis of Caspase 3 expression after SW480 cells treated with different treatments for 48 h. d) Statistical results of c). Data are presented as mean ± SD. n = 3. e) The FCM analysis of apoptotic of SW480 cells subjected to different treatments for 48 h via Annexin V-FITC and PI assays. The sample size was calculated as 10,000 cells using a flow cytometer (events) in each sample. n = 3. *P < 0.05, **P < 0.01, ***P < 0.001. (For interpretation of the references to color in this figure legend, the reader is referred to the Web version of this article.)

3.5. *In vitro gene silencing and inhibition of proliferation and migration*

In *vitro* bioactivity of ERBC was assessed via Western blot. Lipo^{TM}3000-mediated transfection effectively reduced KRAS protein expression by more than 50 % at 20 nM siRNA, establishing a therapeutic siRNA dose of 20 nM. Compared with Lipo^{TM}3000-transfected cells, SW480 cells incubated with ERBC for 48 h presented a 68.27 % decrease in the KRAS protein level and superior efficacy (Fig. 4a and b). Intracellular KRAS proteins serve as molecular switches that induce the activation of the RAS/RAF/ERK signaling pathway, promoting cellular proliferation and survival. Western blot analysis revealed that KRAS silencing successfully inhibited the activity of phosphorylated ERK (pERK), the active molecule of the downstream signaling pathway (Fig. 4c and d). The downregulation of KRAS promotes the re-establishment of normal cellular mechanisms [41]. Herein, the migratory capabilities of the tumor cells were quantified via a Transwell assay. KRAS silencing markedly inhibited the migratory potential of tumor cells (Fig. 4e and f). Additionally, Exo@3BP-CTX significantly decreased the migratory ability of the cells, possibly due to the cytotoxicity of 3BP. The horizontal migratory capacity was further assessed through wound healing assays for 48 h. The results showed that the area traversed by the PBS-treated SW480 cells was 3.42-fold greater than that of the ERBC-treated cells (Fig. 4g and h).

3.6. *Starvation therapy for tumor cells in vitro*

3BP acts as a superior respiratory inhibitor primarily by inhibiting the cellular glycolytic pathway. 3BP can inhibit HK-II and GAPDH, key enzymes of the glycolytic and mitochondrial respiratory pathways [42]. In this study, the cytotoxic impact of 3BP on cells with KRAS mutations was evaluated via the CCK-8 assay. Treatment with 10 μg ml^{-1} 3BP inhibited SW480 cells in a time-dependent manner, leading to a 67.20 % reduction in cell viability after 48 h (Fig. S9). Conversely, 15 μg ml^{-1} 3BP had minimal effect on NCM460 cells. Therefore, 10 μg ml^{-1} 3BP treatment was selected to ensure respiratory depression and minimize off-target effects. Notably, 2-DG (500 μg ml^{-1}), as a typical inhibitor of glycolysis, was used as a positive control. 3BP treatment reduced HK-II and GAPDH expression to 62.41 % and 50.32 %, respectively, in the

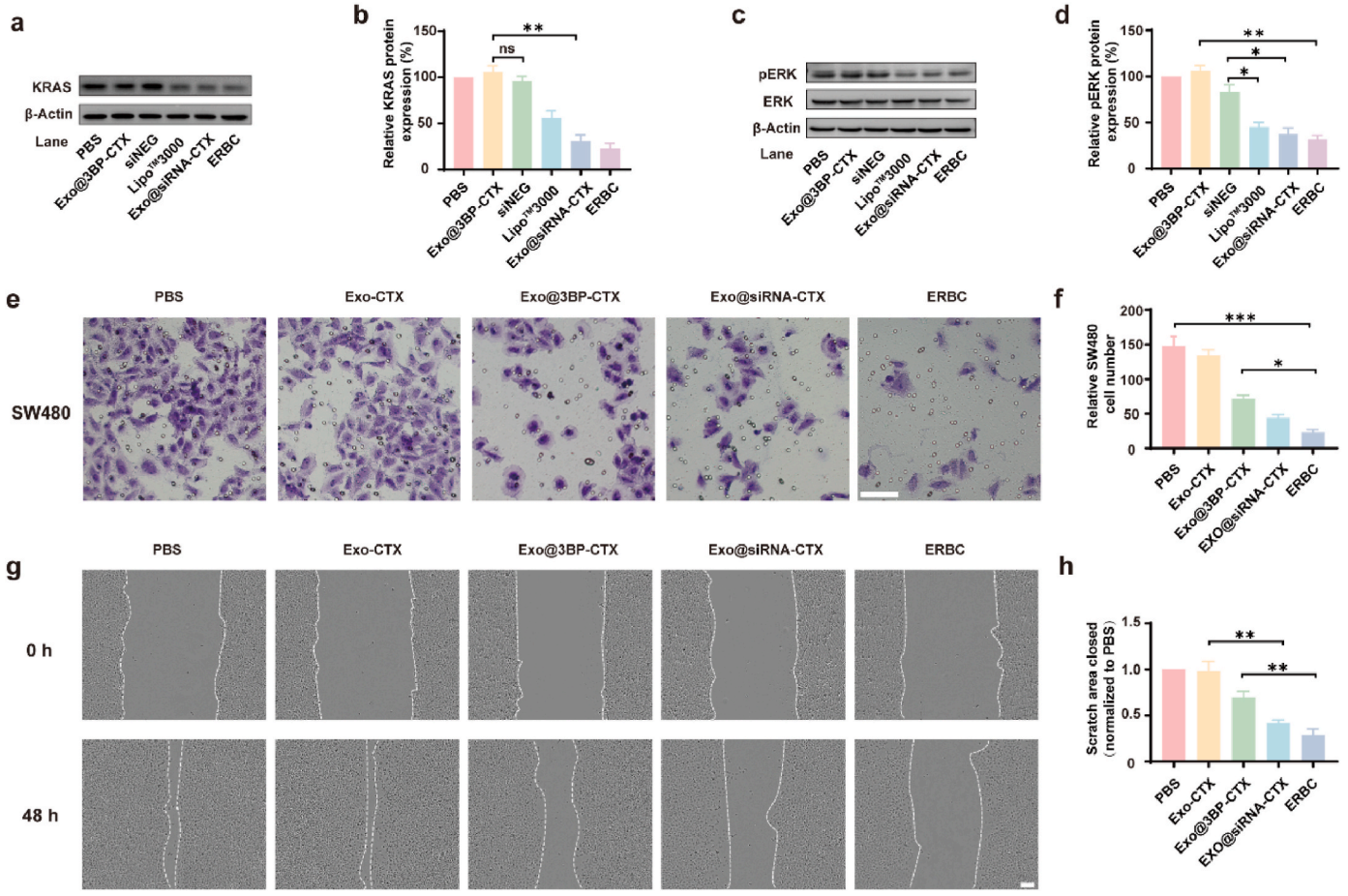

Fig. 4. In *vitro* cell activity and KRAS silencing. a), c) The expression level of KRAS and pERK in SW480 cells was down regulated as determined by Western blotting after the indicated treatments for 48 h. b), d) Statistical analysis of KRAS and pERK protein expression; the data are shown as the mean ± SD. e) Results of the Transwell assay for the SW480 cells after the indicated treatments for 48 h and f) The corresponding relative quantification of the cell number. The data are presented as the mean ± SD. Scale bar: 50 μm. g) The scratch assay showing the closed area by the SW480 cells (between two white lines) after different treatments. h) The representative images and the relative quantification of the scratch area. Data are presented as mean ± SD. Scale bar: 200 μm. (n = 3). Ns: not significant, *P < 0.05, **P < 0.01, ***P < 0.001.

ERBC group (Fig. 5a). Cancer cells obtain energy through glycolysis, indicating that changes in lactate and ATP, the end products and intermediate metabolites of glycolysis, can directly alter the energy supply [43]. In this study, lactate and ATP assay kits were used to detect lactate and ATP contents in SW480 cells. ERBC or Exo@3BP-CTX treatment significantly reduced the lactate and ATP levels in the cells (Fig. 5g and h), reflecting the effect of 3BP. However, this Exo@siRNA-CTX did not affect HK-II and GAPDH expression (Fig. 5a and c). Research has revealed that the upregulation of GLUT1, a KRAS-dependent gene, is associated with increased glucose uptake and glycolysis in KRAS-mutant tumors [44,45]. Therefore, inhibiting KRAS may affect glucose uptake. 3BP targets glycolysis, potentially reducing tumor cell hypoxia. HIF-1α plays a pivotal role in regulating the pro-proliferative effects induced by the hypoxic pathway, predominantly responding to the intracellular hypoxic environment [46]. 3BP treatment can alleviate the hypoxic internal environment of cancer cells [42,47]. Herein, GLUT1 and hypoxia-inducible factor 1α (HIF-1α) expression in SW480 cells after 48h of treatment were assessed via protein blotting. Results showed that Exo@siRNA-CTX and ERBC treatments suppressed GLUT1 expression (Fig. 5d). The above findings suggest that Exo@siRNA-CTX can induce cancer cell starvation. Moreover, combining KRAS siRNA with 3BP can intensify the effects of starvation therapy on tumors.

3.7. Starved cells increase autophagy and promote apoptosis after ERBC treatment

Cellular starvation stimulates autophagy, a process associated with self-protective balance mechanisms [48]. Nonetheless, the overactivation of autophagy associated with the activation of autophagy receptor proteins is depleted, shifting the balance of autophagic regulation from cytoprotective to cytotoxic, thus facilitating tumor cell death [49]. Autophagy produces acidic vesicular autophagosomes through lysosomal phagocytosis and degradation of some of its components. These autophagosomes can be detected via monodanoyl cadaverine (MDC) staining. Herein, the green fluorescence was very weak or absent in the Exo@siRNA-CTX, Exo-CTX, and PBS groups and stronger in the Exo@3BP-CTX and ERBC groups (Fig. 5l). In addition, TEM is the gold standard for visualizing the accumulation of autophagic vesicles within cells. In this study, these vesicles were significantly accumulated in the ERBC compared with the Exo@3BP-CTX group (Fig. 5m). LC 3-I is converted to LC 3-II during autophagy activation, while the autophagy substrate P62 is specifically degraded. Compared with the PBS group, LC3-II/LC3-I ratio increased in the ERBC group by 1.89-fold while P62 decreased to 49.98 % (Fig. 5i). Compared with Exo@3BP-CTX, ERBC increased the LC3-II/LC3-I ratio (Fig. 5k). These findings indicate that the combination therapeutic strategy enhances tumor starvation and autophagic activity. Apoptosis was assessed via the Annexin V-FITC/PI staining methodology. About 75.90 % of the cells in the ERBC-treated

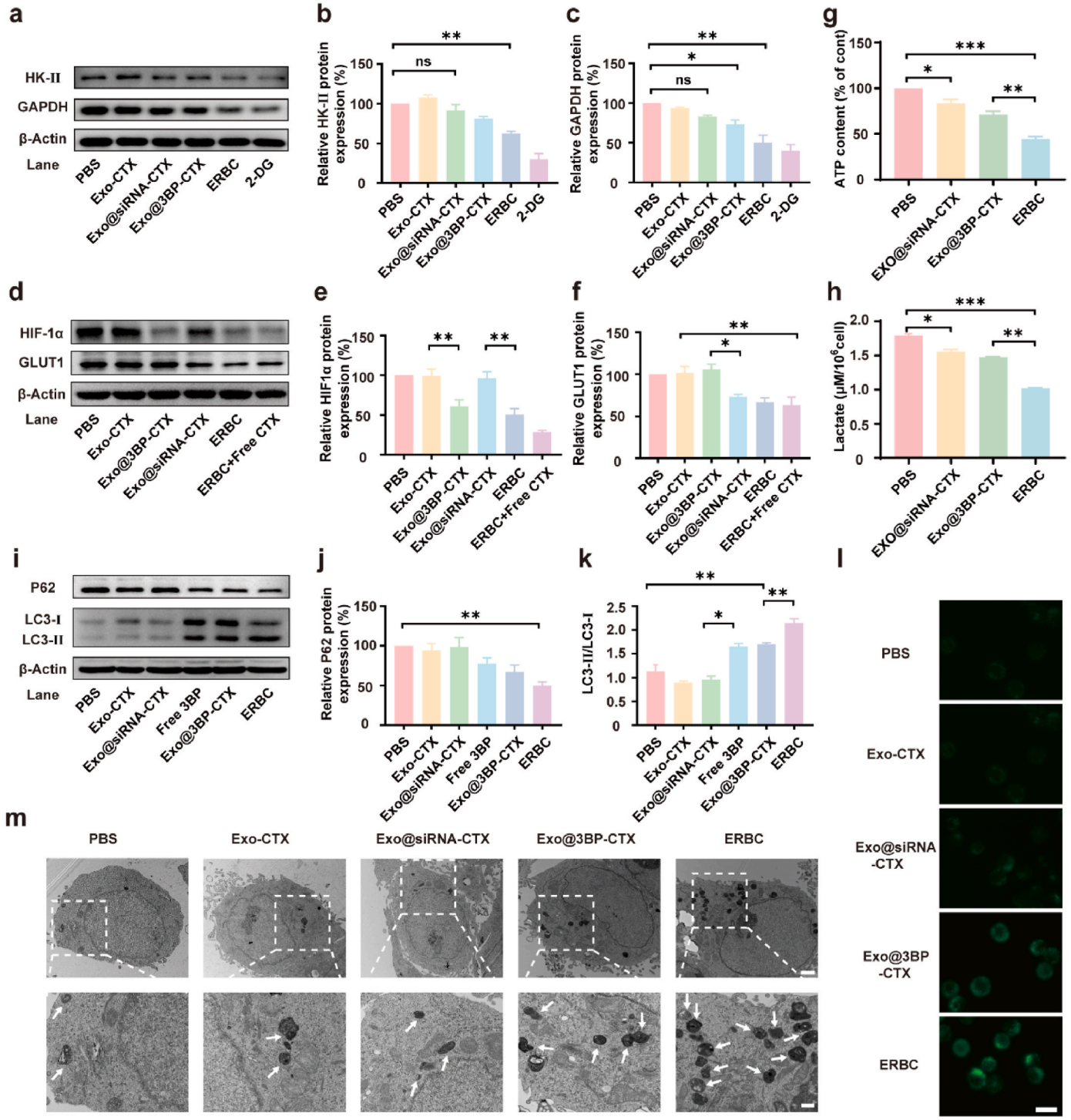

Fig. 5. ERBC induces the starvation in KRAS-mutant tumors to promote autophagy. a) The expression of HK-II in SW480 cells treated with 48 h, as determind by the Western blot analysis, in which GAPDH served as the house keeping gene. b), c) Statistical results of a). The data are shown as the mean ± SD. d) Western blot analysis of HIF-1α and GLUT1 levels after SW480 cells were subjected to different treatments for 48 h. e), f) Statistical results of d). The data are shown as the mean ± SD. i) Western blot analysis of LC3-I, LC3-II and P62 levels after SW480 cells were subjected to different treatments for 48 h. j), k) Statistical results of i). The data are shown as the means ± SD. g) Intracellular lactate levels after SW480 cells were incubated with Exo@siRNA-CTX, Exo@3BP-CTX or ERBC NPs for 48 h. Data are presented as the mean ± SD. h) Intracellular ATP levels in SW480 cells incubated with Exo@siRNA-CTX, Exo@3BP-CTX NPs or ERBC NPs for 48 h. Data are expressed as the mean ± SD. m) TEM image showing the formation of autophagosomes after 48 h of treatment in SW480 cells subjected to different treatments; scale bar:2 μm. Enlarged magnification of the TEM image; typical structures of autophagosomes are indicated with white arrows; scale bar: 500 nm. l) MDC-stained fluorescence images of SW480 cells incubated with different treatments for 48 h; scale bar: 50 μm. n = 3. Ns: not significant, *P < 0.05, **P < 0.01, ***P < 0.001.

cohort underwent apoptosis, higher than the percentage in the Exo@3BP-CTX group (Fig. 3e). The western blot results revealed that the Caspase-3 protein had a similar synergistic effect (Fig. 3c). Studies have shown that 3BP induces autophagy via energy deprivation. This process is augmented by the co-application of KRAS-siRNA. In this study, free 3BP or Exo@3BP-CTX increased cellular autophagy. Besides, the exosome-encapsulated drugs did not decrease the efficiency of drug.

3.8. KRAS silencing restores cetuximab chemosensitivity in colorectal cancer

Cetuximab binds to the extracellular domain of EGFR with higher affinity than its natural ligands (EGF, TGFα, amphiregulin, and epiregulin) and inhibits the autophosphorylation of its tyrosine kinase-dependent signaling pathway [50]. Cellular experiments demonstrated a statistically significant difference in cytotoxicity between the Exo@siRNA-CTX and Exo@siRNA-CTX + free CTX groups. Specifically, the cell death rate in the Exo@siRNA-CTX + free CTX group was 1.57-fold higher than that in the Exo@siRNA-CTX group, suggesting that CTX enhanced the cytotoxicity of KRAS-siRNA in *vitro* (Fig. 3b). Complementary in *vivo* studies also revealed that concurrent treatment with Exo@siRNA-CTX and intravenous free CTX (5 mg ml^{-1}) effectively suppressed tumor proliferation compared with Exo@siRNA-CTX treatment (Fig. 6b and c). This enhanced therapeutic outcome was attributed to the restoration of CTX sensitivity, which hinders the proliferation of KRAS-mutant colorectal cancer cells. The survival rate of SW480 cells in the ERBC + Free CTX treatment was 27.06 %, greater than the combined cell survival rates of Exo@siRNA-CTX + Free CTX and Exo@3BP-CTX alone (Fig. 3b). Furthermore, the combination treatment enhanced energy deprivation in mutant cells and induced death-promoting autophagy. However, PBS, Exo, or Exo-CTX showed no cytotoxic effects after treatment for 48 h (Fig. 3a, b, and 3e), indicating that the Exo-CTX based vector has high biosafety.

3.9. In vivo anti-tumor evaluation of subcutaneous tumors in nude mice

In *vivo* anti-tumor efficacy was assessed using a subcutaneous tumor-forming model of nude mice inoculated with SW480 cells. The treatment regimen is depicted in (Fig. 6a). The therapeutic impact in *vivo* was determined by tracking changes in tumor volume among various treatment groups. Compared with the control group, the tumor volume in the Exo@siRNA-CTX group was reduced by 2.49-fold (Fig. 6d). Furthermore, ERBC + Free CTX and Exos@3BP-CTX decreased the tumor volume, especially after ERBC + Free CTX treatment (Fig. 6c and d). Immunohistochemical analysis revealed that the exosome delivery system effectively achieved in *vivo* knockdown of the KRAS oncogene via KRAS-siRNA (Fig. 6b). These results were visually represented in tumor images (Fig. 6c). In *vivo* immunohistochemical assessments were conducted using isolated tumor samples via H&E staining and Ki67 labeling. Results demonstrated that the ERBC significantly suppressed tumor proliferation and increased apoptosis within neoplastic tissues (Fig. 6b). Apoptosis was highest in the ERBC + Free CTX group (Fig. 6f), consistent with in *vitro* assays. Besides, Western blotting showed that autophagy levels were significantly increased in the ERBC + Free CTX group and the Exo@3BP-CTX group (Fig. 6e). Caspase 3 expression in the treatment group was 3.48-fold higher than in the PBS group (Fig. 6h). Similarly, statistical analysis revealed that the LC3-II/LC3-I ratio was 1.76-fold higher in the treatment group than in the PBS group (Fig. 6g). A significant increase in pro-death autophagy was observed in both the ERBC and Exo@3BP-CTX treatment groups. Notably, the LC3-II/LC3-I ratio in the ERBC group was 1.44-fold higher than that in the Exo@3BP-CTX group (Fig. 6g). These findings further suggest that siRNA-based combination therapy enhances the starvation effect of 3BP, thereby promoting tumor autophagy. Moreover, body weight did not significantly change over 21 days (Fig. S10). Also, liver and kidney function did not significantly change (Fig. S11). Additionally, H&E staining of visceral organ sections revealed no evidence of organ damage after 21 days of treatment (Fig. S12), indicating that exosome-mediated drug delivery was well tolerated in *vivo*.

4. Conclusion

ERBC nanomaterials were developed using an exosome platform to encapsulate KRAS siRNA and 3BP via electroporation and explore therapeutic strategies for refractory KRAS-mutant colorectal cancer. An in *vivo* biodistribution study of the nanomaterials revealed that CTX could specifically target tumor cells expressing high levels of EGFR when modified with DSPE-PEG-NHs as linkers. Furthermore, these nanomaterials effectively silenced the KRAS gene ex *vivo*, suggesting a potential treatment for EGFR inhibitor-resistant KRAS-mutant colorectal cancer. Also, Exo@siRNA-CTX combined with free CTX enhanced cytotoxic effects. The silencing of KRAS successfully resensitized the cells to CTX. Additionally, ERBC significantly reduced intracellular lactate and ATP levels compared with Exo@3BP-CTX alone, indicating that KRAS siRNA combination therapy enhances the effects of 3BP starvation therapy. ERBC also inhibited tumor migration and invasion in *vitro* and in *vivo*, induced autophagy, and increased apoptosis in cancer cells. These findings suggest that ERBC is a promising and effective antitumor regimen for KRAS-mutant tumors, offering a novel approach for the treatment of drug-resistant KRAS-mutated cancers.

5. Discussion

Patients with CRC harboring KRAS mutations generally have a poor prognosis. Despite significant advancements in treatment strategies, including improved surgical techniques and optimized adjuvant therapies, CRC-related mortality remains high due to postoperative recurrence and metastasis [51]. This highlights the critical role of KRAS mutations in CRC and underscores their prominence as a key research focus. Researchers have focused on developing direct KRAS-targeting strategies, including covalent inhibitors against $KRAS^{G12C}$ and agents targeting the RAS-binding pocket [2]. Indirect KRAS inhibition strategies encompass nucleotide cycling inhibitors, interference with KRAS processing and membrane localization, and targeting downstream signaling pathways [2,4]. Additionally, novel therapeutic strategies, including immune checkpoint inhibitors and anti-KRAS vaccines, are being investigated. However, the clinical efficacy of these approaches remains limited, largely due to the challenges of monotherapy and the development of drug resistance. RNAi is a promising therapeutic strategy for regulating disease-associated gene expression, providing an effective approach for targeting KRAS-mutated tumors that are refractory to conventional treatments.

KRAS mutations impair GTP hydrolysis and/or enhance nucleotide exchange, leading to an accumulation of KRAS in its active state and persistent activation of downstream signaling pathways. The KRAS protein acts as a “molecular switch” that cycles between a GDP-bound inactive state and a GTP bound active state [51].GTP binding facilitates interactions with downstream effectors, thereby activating key oncogenic pathways, including the rapidly accelerated fibrosarcoma (RAF)-mitogen-activated protein kinase kinase (MEK)-extracellular signal-regulated kinase (ERK) cascade and the phosphatidylinositol 3-kinase (PI3K)-protein kinase B (AKT)-mechanistic target of rapamycin (mTOR) pathway, both of which drive tumor growth and survival [52].

In this study, we employed a combinatorial therapeutic strategy integrating siRNA-based RNAi therapy with the glycolysis inhibitor 3-bromopyruvate (3BP) to enhance the treatment efficacy against KRAS-mutated tumors. KRAS mutations significantly alter intracellular glucose and lipid metabolism, notably upregulating GLUTs expression, thereby increasing the glycolytic capacity of cancer cells. This metabolic adaptation confers heightened susceptibility to glycolysis inhibitors such as 3BP. By directly suppressing the expression of mutant KRAS, our approach reduced the accumulation of its active form, thereby inhibiting

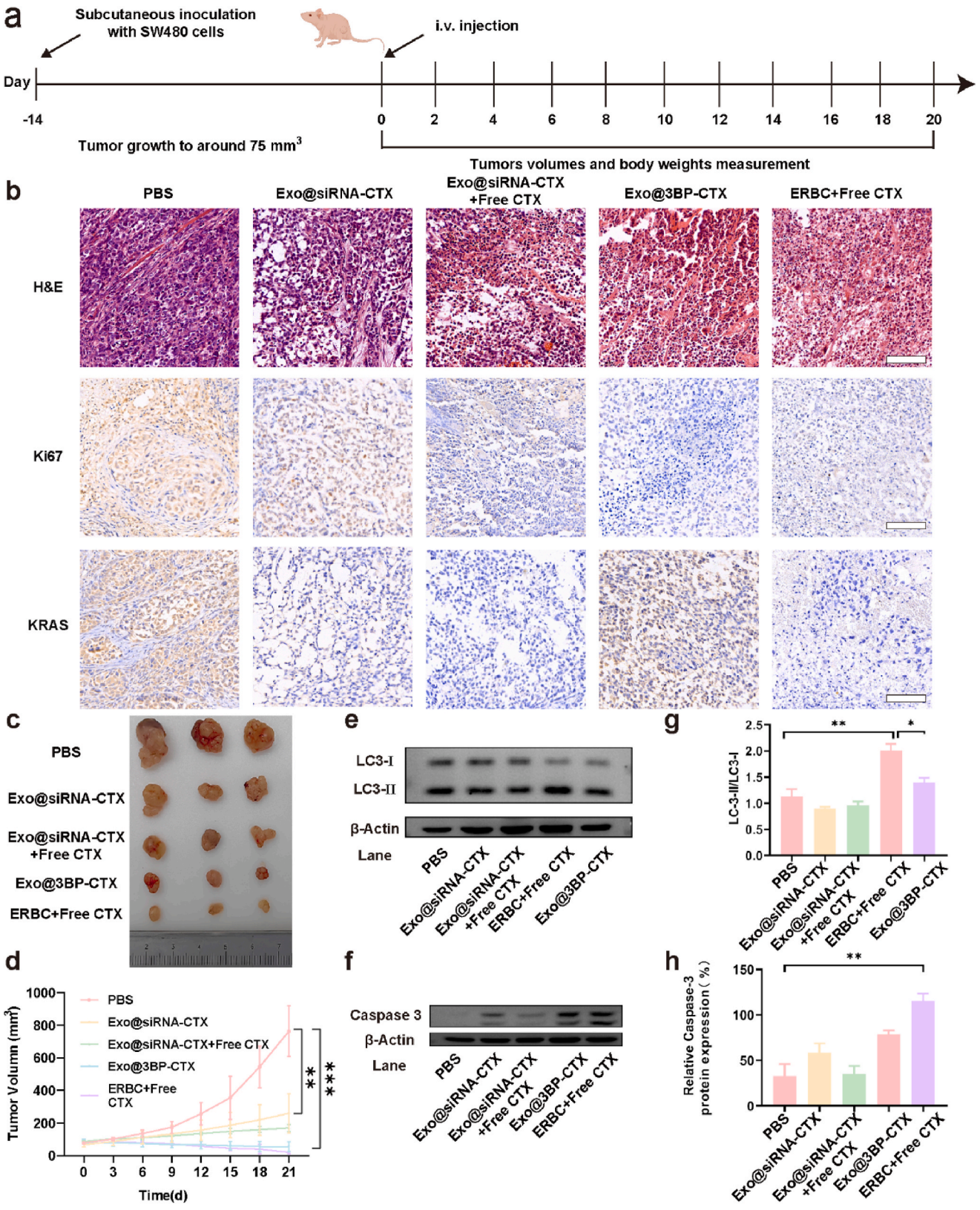

Fig. 6. In *vivo* antitumor analysis, autophagy, and apoptosis levels in the subcutaneous tumors. a) The schematic representation of the treatment protocols for SW480 subcutaneous tumor inoculation and drug delivery protocols. Different treatments (~10^9 exosomes per rat equiv) were intravenously injected (i. v.) into hormone-treated mice once the tumor volume increased to 75 mm^3. The tumor volume and body weight of each mouse were monitored and recorded on days 0, 3, 6, 9, 12, 15, 18 and 21. b) Histological analysis of the tumor from all groups was examined using H&E, KRAS and Ki 67 analyses. Scale bar: 100 μm. c) The tumor images and d) tumor growth curve after treatment with PBS, Exo@siRNA-CTX, Exo@siRNA-CTX + Free CTX, Exo@3BP-CTX and ERBC + Free CTX, respectively. Data are means ± SD (n = 3). e) Western blot analysis of the levels of LC3-I and C3-II in the tumor tissues of the mice after the indicated treatments. f) Western blot analysis of caspase 3 levels in the tumor tissues of mice after the indicated treatments. g), h) Statistical results of e) and f). Data are means ± SD (n = 3). *P < 0.05 **P < 0.01.

cancer cell proliferation and migration. Moreover, this inhibition modulated glucose metabolism in KRAS-overexpressing cells, as evidenced by decreased GLUTs expression and reduced glucose uptake. Consequently, this synergistic strategy potentiated the starvation therapy effect of 3BP, exerting dual anti-tumor actions while minimizing toxicity to normal cells (Fig. 7). Starvation therapy induces autophagy-mediated cell death in tumor cells. In our study, Exo@siRNA-CTX treatment had a minimal effect on autophagy induction. However, when combined with ERBC, we observed a significant hyperactivation of autophagy, further amplifying the therapeutic response.

Exosomes, as endogenous vesicles, possess distinct advantages compared to synthetic inorganic materials: 1) Exosomes derived from normal cells exhibit superior biocompatibility and lower immunogenicity. 2) They have broad biological distribution and the capability to traverse the blood-brain barrier. 3) Exosomes effectively encapsulate proteins, miRNAs, siRNAs, and other therapeutic molecules, shielding them from enzymatic degradation [53]. Given these advantages, we selected exosomes as delivery vehicles for KRAS-siRNA and 3BP. However, the clinical translation of exosome-based therapies remains hindered by suboptimal targeting efficiency. Enhancing the expression of target ligands on exosomes surfaces can improve their specificity for cell- or tissue-selective delivery. To address this limitation, we functionalized the exosome membrane with cetuximab, a monoclonal antibody, facilitating precise drug delivery to EGFR-overexpressing tumors via receptor-ligand interactions. Our *in vivo* experiments demonstrated that ERBC preferentially accumulated at the tumor site within 48 h. After 21 days of intravenous administration, the tumor volume in the PBS group was 39.56 times greater than that in the ERBC-treated group, highlighting the significant anti-tumor efficacy of this approach. The exosomes used in this study were derived from HEK293T cells, which served as producer cells. However, it is important to acknowledge that nude mouse models do not fully recapitulate drug pharmacokinetics within an intact immune system. Previous studies have reported that $CD47^{+}$ exosomes derived from fibroblast cultures exhibit reduced clearance by monocytes and macrophages [8]. Given the complexity of the human immune system, further research is warranted to explore the feasibility of employing natural exosomes as drug carriers in clinical applications.

Nanomedicine-based strategies for tumor therapy primarily involve the precise delivery of anticancer agents via various carriers, modulation of the tumor microenvironment (TME) using nanoparticles to stimulate anti-tumor immune responses and enhance immunotherapy efficacy, utilization of nanoparticles as radiosensitizers, and application of photodynamic therapy (PDT) and photothermal therapy (PTT) as innovative light-based cancer treatments. Both viral and non-viral vectors are employed for the intracellular delivery of genetic material in gene therapy. Two primary strategies are employed in the treatment of KRAS-mutated tumors: (1) Gene therapy, which utilizes siRNA/miRNA or the CRISPR-Cas13a system delivered via different carriers to target overexpressed KRAS proteins [36,54]; and (2) enhancement of therapeutic efficacy through improved in *vivo* delivery of conventional chemotherapeutic agents such as oxaliplatin, or through combination therapy integrating chemotherapy with immunotherapy. In this study, we developed ERBC by combining gene therapy with enhanced starvation therapy [55,56]. Our findings suggest that combining ERBC with cetuximab enhances therapeutic efficacy and restores cetuximab sensitivity. For refractory KRAS-mutated tumors, multi-drug combination therapy may provide an effective strategy for tumor suppression.

CRediT authorship contribution statement

Yurong Xiang: Writing – review & editing, Writing – original draft, Validation, Methodology, Data curation. **Qiang Liu:** Writing – original draft, Resources, Methodology, Investigation, Data curation. **Kang Liu:** Writing – review & editing, Project administration, Methodology, Formal analysis, Conceptualization. **Liuxian Chen:** Writing – review & editing, Visualization, Validation, Software, Resources, Investigation. **Fengjiao Chen:** Writing – review & editing, Visualization, Project administration, Conceptualization. **Tao Li:** Writing – review & editing, Software, Methodology, Formal analysis. **Siqi Li:** Writing – review &

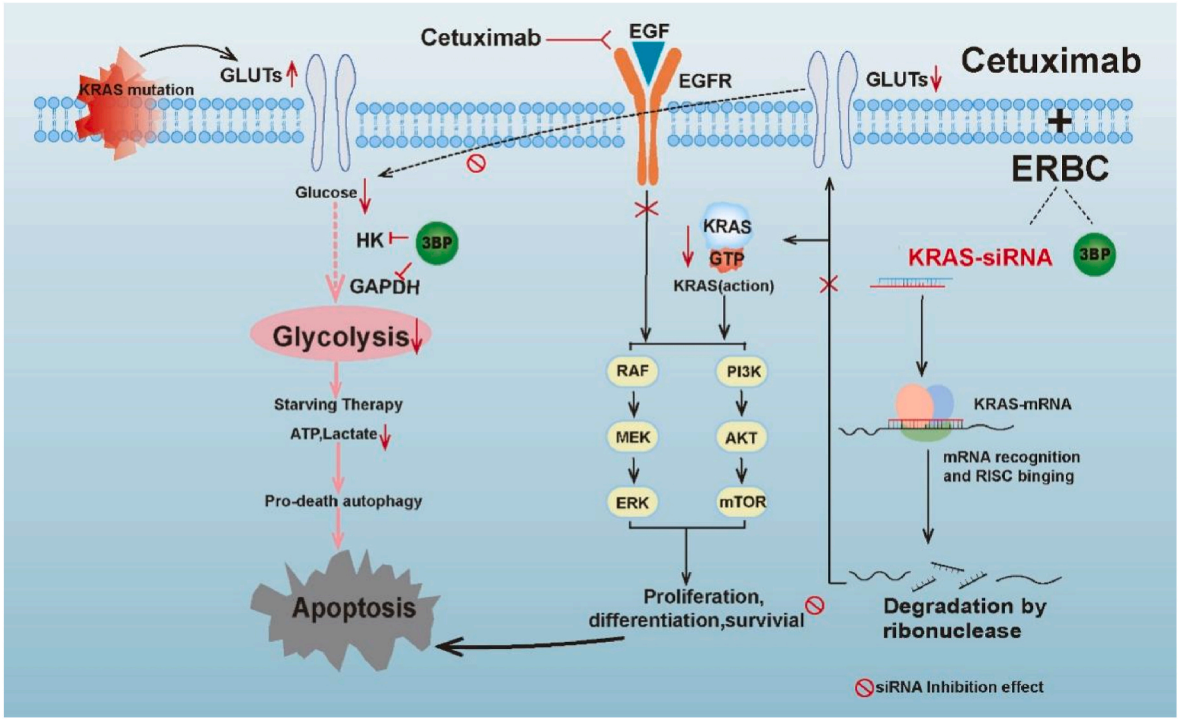

Fig. 7. A schematic diagram about the central role of co-treatment with KRAS-siRNA and 3BP in migration inhibition and pro-death autophagy. Combinative treatment of ERBC and cetuximab is sensitive to KRAS mutant CRC cells by Inhibition of mutated KRAS expression and enhanced hunger therapy by 3BP pathway and suppressing cancer migration.

editing, Software. **Qiang Yu:** Writing – original draft, Resources, Data curation. **Quan Lv:** Writing – review & editing, Visualization, Validation, Software. **Zheng Xiang:** Writing – review & editing, Supervision, Project administration, Funding acquisition, Conceptualization.

Funding sources

Funding:This study was supported by the Natural Science Foundation of Chongqing, China (cstc2019jcyj-msxmX0054) and the Science and Technology Planning Project of Yuzhong District of Chongqing City (20210115).

Declaration of competing interest

The authors declare that they have no known competing financial interests or personal relationships that could have appeared to influence the work reported in this paper.

Appendix A. Supplementary data

Supplementary data to this article can be found online at https://doi.org/10.1016/j.mtbio.2025.101732.

Data availability

No data was used for the research described in the article.

References

[1] M.B. Ryan, R.B. Corcoran, Therapeutic strategies to target RAS-mutant cancers, Nat. Rev. Clin. Oncol. 15 (11) (2018) 709–720.
[2] R. Dienstmann, K. Connor, A.T. Byrne, Precision therapy in RAS mutant colorectal cancer, Gastroenterology 158 (4) (2020) 806–811.
[3] S. Misale, R. Yaeger, S. Hobor, E. Scala, M. Janakiraman, D. Liska, E. Valtorta, R. Schiavo, M. Buscarino, G. Siravegna, K. Bencardino, A. Cercek, C.T. Chen, S. Veronese, C. Zanon, A. Sartore-Bianchi, M. Gambacorta, M. Gallicchio, E. Vakiani, V. Boscaro, E. Medico, M. Weiser, S. Siena, F. Di Nicolantonio, D. Solit, A. Bardelli, Emergence of KRAS mutations and acquired resistance to anti-EGFR therapy in colorectal cancer, Nature 486 (7404) (2012) 532–536.
[4] G. Zhu, L. Pei, H. Xia, Q. Tang, F. Bi, Role of oncogenic KRAS in the prognosis, diagnosis and treatment of colorectal cancer, Mol. Cancer 20 (1) (2021) 143.
[5] B. Hu, L. Zhong, Y. Weng, L. Peng, Y. Huang, Y. Zhao, X.J. Liang, Therapeutic siRNA: state of the art, Signal Transduct Target Ther 5 (1) (2020) 101.
[6] R.R. Nikam, K.R. Gore, Journey of siRNA: clinical developments and targeted delivery, Nucleic Acid Ther 28 (4) (2018) 209–224.
[7] Z. Fu, X. Zhang, X. Zhou, U. Ur-Rehman, M. Yu, H. Liang, H. Guo, X. Guo, Y. Kong, Y. Su, Y. Ye, X. Hu, W. Cheng, J. Wu, Y. Wang, Y. Gu, S.F. Lu, D. Wu, K. Zen, J. Li, C. Yan, C.Y. Zhang, X. Chen, In vivo self-assembled small RNAs as a new generation of RNAi therapeutics, Cell Res. 31 (6) (2021) 631–648.
[8] S. Kamerkar, V.S. LeBleu, H. Sugimoto, S. Yang, C.F. Ruivo, S.A. Melo, J.J. Lee, R. Kalluri, Exosomes facilitate therapeutic targeting of oncogenic KRAS in pancreatic cancer, Nature 546 (7659) (2017) 498–503.
[9] Y. Tong, W.Q. Gao, Y. Liu, Metabolic heterogeneity in cancer: an overview and therapeutic implications, Biochim. Biophys. Acta Rev. Canc 1874 (2) (2020) 188421.
[10] S. Ganapathy-Kanniappan, J.F. Geschwind, Tumor glycolysis as a target for cancer therapy: progress and prospects, Mol. Cancer 12 (2013) 152.
[11] K. Kawada, Y. Nakamoto, M. Kawada, K. Hida, T. Matsumoto, T. Murakami, S. Hasegawa, K. Togashi, Y. Sakai, Relationship between 18F-fluorodeoxyglucose accumulation and KRAS/BRAF mutations in colorectal cancer, Clin. Cancer Res. 18 (6) (2012) 1696–1703.
[12] J. Yun, C. Rago, I. Cheong, R. Pagliarini, P. Angenendt, H. Rajagopalan, K. Schmidt, J.K. Willson, S. Markowitz, S. Zhou, L.A. Diaz Jr., V.E. Velculescu, C. Lengauer, K.W. Kinzler, B. Vogelstein, N. Papadopoulos, Glucose deprivation contributes to the development of KRAS pathway mutations in tumor cells, Science 325 (5947) (2009) 1555–1559.
[13] T. Fan, G. Sun, X. Sun, L. Zhao, R. Zhong, Y. Peng, Tumor energy metabolism and potential of 3-bromopyruvate as an inhibitor of aerobic glycolysis: implications in tumor treatment, Cancers (Basel) 11 (3) (2019).
[14] Z. Wang, H. Li, W. She, X. Zhang, Y. Liu, Y. Liu, P. Jiang, 3-Bromopyruvate-Loaded Ti(3)C(2) MXene/Cu(2)O nanosheets for photoacoustic imaging-guided and hypoxia-relieving enhanced photothermal/chemodynamic therapy, Anal. Chem. 95 (2) (2023) 1710–1720.
[15] S. Yadav, S.K. Pandey, A. Kumar, P.K. Kujur, R.P. Singh, S.M. Singh, Antitumor and chemosensitizing action of 3-bromopyruvate: implication of deregulated metabolism, Chem. Biol. Interact. 270 (2017) 73–89.
[16] Y.H. Ko, B.L. Smith, Y. Wang, M.G. Pomper, D.A. Rini, M.S. Torbenson, J. Hullihen, P.L. Pedersen, Advanced cancers: eradication in all cases using 3-bromopyruvate therapy to deplete ATP, Biochem. Biophys. Res. Commun. 324 (1) (2004) 269–275.
[17] A.F. Abdel-Wahab, W. Mahmoud, R.M. Al-Harizy, Targeting glucose metabolism to suppress cancer progression: prospective of anti-glycolytic cancer therapy, Pharmacol. Res. 150 (2019) 104511.
[18] S.M. El Sayed, Enhancing anticancer effects, decreasing risks and solving practical problems facing 3-bromopyruvate in clinical oncology: 10 years of research experience, Int. J. Nanomed. 13 (2018) 4699–4709.
[19] R. Kalluri, V.S. LeBleu, The biology, function, and biomedical applications of exosomes, Science 367 (6478) (2020).
[20] H. Tao, H. Xu, L. Zuo, C. Li, G. Qiao, M. Guo, L. Zheng, M. Leitgeb, X. Lin, Exosomes-coated bcl-2 siRNA inhibits the growth of digestive system tumors both in vitro and in vivo, Int. J. Biol. Macromol. 161 (2020) 470–480.
[21] G. Jia, Y. Han, Y. An, Y. Ding, C. He, X. Wang, Q. Tang, NRP-1 targeted and cargo-loaded exosomes facilitate simultaneous imaging and therapy of glioma in vitro and in vivo, Biomaterials 178 (2018) 302–316.
[22] L. Mashouri, H. Yousefi, A.R. Aref, A.M. Ahadi, F. Molaei, S.K. Alahari, Exosomes: composition, biogenesis, and mechanisms in cancer metastasis and drug resistance, Mol. Cancer 18 (1) (2019) 75.
[23] S.H. Tseng, M.Y. Chou, I.M. Chu, Cetuximab-conjugated iron oxide nanoparticles for cancer imaging and therapy, Int. J. Nanomed. 10 (2015) 3663–3685.
[24] C.M. Van Wagoner, F. Rivera-Escalera, N.C. Jaimes-Delgadillo, C.C. Chu, C.S. Zent, M.R. Elliott, Antibody-mediated phagocytosis in cancer immunotherapy, Immunol. Rev. 319 (1) (2023) 128–141.
[25] M. Ritchie, L. Tchistiakova, N. Scott, Implications of receptor-mediated endocytosis and intracellular trafficking dynamics in the development of antibody drug conjugates, mAbs 5 (1) (2013) 13–21.
[26] G. Hanck-Silva, L.N. Fatori Trevizan, R. Petrilli, F.T. de Lima, J.O. Eloy, M. Chorilli, A critical review of properties and analytical/bioanalytical methods for characterization of cetuximab, Crit. Rev. Anal. Chem. 50 (2) (2020) 125–135.
[27] Y.S. Cho, T.J. Yoon, E.S. Jang, K. Soo Hong, S. Young Lee, O. Ran Kim, C. Park, Y. J. Kim, G.C. Yi, K. Chang, Cetuximab-conjugated magneto-fluorescent silica nanoparticles for in vivo colon cancer targeting and imaging, Cancer Lett. 299 (1) (2010) 63–71.
[28] A.K. Mehata Vikas, M.N.L. Suseela, C. Behera, P. Kumari, S.K. Mahto, M.S. Muthu, Chitosan-alginate nanoparticles of cabazitaxel: design, dual-receptor targeting and efficacy in lung cancer model, Int. J. Biol. Macromol. 221 (2022) 874–890.
[29] E.V. Batrakova, M.S. Kim, Using exosomes, naturally-equipped nanocarriers, for drug delivery, J. Contr. Release 219 (2015) 396–405.
[30] S. El-Andaloussi, Y. Lee, S. Lakhal-Littleton, J. Li, Y. Seow, C. Gardiner, L. Alvarez-Erviti, I.L. Sargent, M.J. Wood, Exosome-mediated delivery of siRNA in vitro and in vivo, Nat. Protoc. 7 (12) (2012) 2112–2126.
[31] S. Pan, Y. Zhang, M. Huang, Z. Deng, A. Zhang, L. Pei, L. Wang, W. Zhao, L. Ma, Q. Zhang, D. Cui, Urinary exosomes-based engineered nanovectors for homologously targeted chemo-chemodynamic prostate cancer therapy via abrogating EGFR/AKT/NF-kB/IkB signaling, Biomaterials 275 (2021) 120946.
[32] C. Feng, Z. Xiong, C. Wang, W. Xiao, H. Xiao, K. Xie, K. Chen, H. Liang, X. Zhang, H. Yang, Folic acid-modified Exosome-PH20 enhances the efficiency of therapy via modulation of the tumor microenvironment and directly inhibits tumor cell metastasis, Bioact. Mater. 6 (4) (2021) 963–974.
[33] W. Huang, M. Qu, L. Li, T. Liu, M. Lin, X. Yu, SiRNA in MSC-derived exosomes silences CTGF gene for locomotor recovery in spinal cord injury rats, Stem Cell Res. Ther. 12 (1) (2021) 334.
[34] G. Singh, A. Mehra, S. Arora, D. Gugulothu, L.K. Vora, R. Prasad, D.K. Khatri, Exosome-mediated delivery and regulation in neurological disease progression, Int. J. Biol. Macromol. 264 (Pt 2) (2024) 130728.
[35] R. Sabra, N. Billa, C.J. Roberts, Cetuximab-conjugated chitosan-pectinate (modified) composite nanoparticles for targeting colon cancer, Int J Pharm 572 (2019) 118775.
[36] S. Bäumer, N. Bäumer, N. Appel, L. Terheyden, J. Fremerey, S. Schelhaas, E. Wardelmann, F. Buchholz, W.E. Berdel, C. Müller-Tidow, Antibody-mediated delivery of anti-KRAS-siRNA in vivo overcomes therapy resistance in colon cancer, Clin. Cancer Res. 21 (6) (2015) 1383–1394.
[37] L. Alvarez-Erviti, Y. Seow, H. Yin, C. Betts, S. Lakhal, M.J. Wood, Delivery of siRNA to the mouse brain by systemic injection of targeted exosomes, Nat. Biotechnol. 29 (4) (2011) 341–345.
[38] B. Dorjsuren, B. Chaurasiya, Z. Ye, Y. Liu, W. Li, C. Wang, D. Shi, C.E. Evans, T. J. Webster, Y. Shen, Cetuximab-Coated thermo-sensitive liposomes loaded with magnetic nanoparticles and doxorubicin for targeted EGFR-expressing breast cancer combined therapy, Int. J. Nanomed. 15 (2020) 8201–8215.
[39] L. Wang, D. Geng, H. Su, Safe and efficient pH sensitive tumor targeting modified liposomes with minimal cytotoxicity, Colloids Surf. B Biointerfaces 123 (2014) 395–402.
[40] J.S. Choi, J.S. Park, Design and evaluation of the anticancer activity of paclitaxel-loaded anisotropic-poly(lactic-co-glycolic acid) nanoparticles with PEGylated chitosan surface modifications, Int. J. Biol. Macromol. 162 (2020) 1064–1075.
[41] P.Y. Chen, M.D. Muzumdar, K.J. Dorans, R. Robbins, A. Bhutkar, A. Del Rosario, P. Mertins, J. Qiao, A.C. Schafer, F. Gertler, S. Carr, T. Jacks, Adaptive and reversible resistance to kras inhibition in pancreatic cancer cells, Cancer Res. 78 (4) (2018) 985–1002.
[42] Y. Deng, P. Song, X. Chen, Y. Huang, L. Hong, Q. Jin, J. Ji, 3-Bromopyruvate-Conjugated nanoplatform-induced pro-death autophagy for enhanced photodynamic therapy against hypoxic tumor, ACS Nano 14 (8) (2020) 9711–9727.

[43] S. Paul, S. Ghosh, S. Kumar, Tumor glycolysis, an essential sweet tooth of tumor cells, Semin. Cancer Biol. 86 (Pt 3) (2022) 1216–1230.
[44] J. Erber, J.D. Steiner, J. Isensee, L.A. Lobbes, A. Toschka, F. Beleggia, A. Schmitt, R. W.J. Kaiser, F. Siedek, T. Persigehl, T. Hucho, H.C. Reinhardt, Dual inhibition of GLUT1 and the ATR/CHK1 kinase Axis displays synergistic cytotoxicity in KRAS-mutant cancer cells, Cancer Res. 79 (19) (2019) 4855–4868.
[45] J. Yun, E. Mullarky, C. Lu, K.N. Bosch, A. Kavalier, K. Rivera, J. Roper, I.I. Chio, E. G. Giannopoulou, C. Rago, A. Muley, J.M. Asara, J. Paik, O. Elemento, Z. Chen, D. J. Pappin, L.E. Dow, N. Papadopoulos, S.S. Gross, L.C. Cantley, Vitamin C selectively kills KRAS and BRAF mutant colorectal cancer cells by targeting GAPDH, Science 350 (6266) (2015) 1391–1396.
[46] G.L. Semenza, HIF-1 and tumor progression: pathophysiology and therapeutics, Trends Mol. Med. 8 (4 Suppl) (2002) S62–S67.
[47] S. Marrache, S. Dhar, The energy blocker inside the power house: mitochondria targeted delivery of 3-bromopyruvate, Chem. Sci. 6 (3) (2015) 1832–1845.
[48] W. Ornatowski, Q. Lu, M. Yegambaram, A.E. Garcia, E.A. Zemskov, E. Maltepe, J. R. Fineman, T. Wang, S.M. Black, Complex interplay between autophagy and oxidative stress in the development of pulmonary disease, Redox Biol. 36 (2020) 101679.
[49] E.H. Baehrecke, Autophagy: dual roles in life and death? Nat. Rev. Mol. Cell Biol. 6 (6) (2005) 505–510.
[50] P. Wee, Z. Wang, Epidermal growth factor receptor cell proliferation signaling pathways, Cancers (Basel) 9 (5) (2017).
[51] M. Drosten, M. Barbacid, Targeting the MAPK pathway in KRAS-driven tumors, Cancer Cell 37 (4) (2020) 543–550.
[52] L. Huang, Z. Guo, F. Wang, L. Fu, KRAS mutation: from undruggable to druggable in cancer, Signal Transduct Target Ther 6 (1) (2021) 386.
[53] Z. Zou, H. Li, G. Xu, Y. Hu, W. Zhang, K. Tian, Current knowledge and future perspectives of exosomes as nanocarriers in diagnosis and treatment of diseases, Int. J. Nanomed. 18 (2023) 4751–4778.
[54] X. Zhao, L. Liu, J. Lang, K. Cheng, Y. Wang, X. Li, J. Shi, Y. Wang, G. Nie, A CRISPR-Cas13a system for efficient and specific therapeutic targeting of mutant KRAS for pancreatic cancer treatment, Cancer Lett. 431 (2018) 171–181.
[55] J. Li, S. Ma, Q. Lin, Q. Wang, W. Zhong, C. Wei, J. Liu, J. Chen, D. Wang, W. Tang, T. Luo, Orchestrated copper-loaded nanoreactor for simultaneous induction of cuproptosis and immunotherapeutic intervention in colorectal cancer, Mater Today Bio 29 (2024) 101326.
[56] S. Tummala, K. Gowthamarajan, M.N. Satish Kumar, A. Wadhwani, Oxaliplatin immuno hybrid nanoparticles for active targeting: an approach for enhanced apoptotic activity and drug delivery to colorectal tumors, Drug Deliv. 23 (5) (2016) 1773–1787.